An Alkylated Indacenodithieno[3,2-b]thiophene-Based Nonfullerene Acceptor with High Crystallinity Exhibiting Single Junction Solar Cell Efficiencies Greater than 13% with Low Voltage Losses

Zhuping Fei, Flurin D. Eisner, Xuechen Jiao, Mohammed Azzouzi, Jason A. Röhr, Yang Han,* Munazza Shahid, Anthony S. R. Chesman, Christopher D. Easton, Christopher R. McNeill, Thomas D. Anthopoulos, Jenny Nelson, and Martin Heeney*

A new synthetic route, to prepare an alkylated indacenodithieno[3,2-b]thiophene-based nonfullerene acceptor (C8-ITIC), is reported. Compared to the reported ITIC with phenylalkyl side chains, the new acceptor C8-ITIC exhibits a reduction in the optical band gap, higher absorptivity, and an increased propensity to crystallize. Accordingly, blends with the donor polymer PBDB-T exhibit a power conversion efficiency (PCE) up to 12.4%. Further improvements in efficiency are found upon backbone fluorination of the donor polymer to afford the novel material PFBDB-T. The resulting blend with C8-ITIC shows an impressive PCE up to 13.2% as a result of the higher open-circuit voltage. Electroluminescence studies demonstrate that backbone fluorination reduces the energy loss of the blends, with PFBDB-T/C8-ITIC-based cells exhibiting a small energy loss of 0.6 eV combined with a high J_{SC} of 19.6 mA cm^{-2}.

The development of nonfullerene acceptors (NFAs), which are used to replace fullerene derivatives in organic solar cells (OSCs) due to their extended light absorption and tunable energy levels, has seen impressive progress in the past few years.[1–4] A range of new NFAs with different building blocks and geometrical dimensions has been designed to boost the power conversion efficiency (PCE) of OSCs. Among the highest performing NFAs, linear rod-like acceptor–donor–acceptor (A–D–A) structures incorporating fused ladder-type aromatics have attracted much interest. Common donor units include 4,9-dihydro-s-indaceno[1,2-b:5,6-b']dithiophene (IDT)[5–9] and 6,12-dihydro-dithienoindeno

[2,3-d:2′,3′-d']-s-indaceno[1,2-b:5,6-b']dithiophene (IDTT).[10–18] In both cases, the fused core facilitates π-electron delocalization and improves the π–π stacking between molecules, hence enhancing the intrinsic charge carrier mobility.

In 2015, Zhan and coworkers reported a new NFA, 3,9-bis(2-methylene-(3-(1,1-dicyanomethylene)-indanone))-5,5,11,11-tetrakis(4-hexylphenyl)-dithieno[2,3-d:2′,3′-d']-s-indaceno[1,2-b:5,6-b']dithiophene (ITIC) (**Scheme 1**), which is comprised an electron-donating IDTT-based core flanked by two electron-withdrawing units of 1,1-dicyanomethylene-3-indanone (IC), that exhibited a promising PCE of 6.8% at that time.[10] Since then, many strategies have been applied to modify the structure of ITIC in order to adjust the absorption spectra and energy levels to further improve the PCE, for example, by changing the side chains,[17,18] extending the conjugation length,[19–22] and substituting the end acceptor groups.[13–16] To date, a few systems based on these NFAs have achieved a PCE of over 10%.[5,13–15,18,20,22] However, it is noticeable that in all cases these NFAs incorporate phenylalkyl or thienylalkyl side chains as the solubilizing groups on the fused core. These aryl-based side chains facilitate the synthesis of the IDTT core under Friedel–Crafts conditions via the formation of stable triaryl cations. However, since the nature of the side chains has a

Dr. Z. Fei, Dr. Y. Han, Dr. M. Shahid, Prof. M. Heeney
Department of Chemistry and Centre for Plastic Electronics
Imperial College London
London SW7 2AZ, UK
E-mail: yang.han@tju.edu.cn; m.heeney@imperial.ac.uk
F. D. Eisner, M. Azzouzi, J. A. Röhr, Prof. J. Nelson
Department of Physics and Centre for Plastic Electronics
Imperial College London
London SW7 2AZ, UK

Dr. X. Jiao, Prof. C. R. McNeill
Department of Materials Science and Engineering
Monash University
Victoria 3800, Australia
Dr. A. S. R. Chesman, Dr. C. D. Easton
CSIRO Manufacturing
Ian Wark Laboratories
Clayton, Victoria 3168, Australia
Prof. T. D. Anthopoulos
Division of Physical Sciences and Engineering
King Abdullah University of Science and Technology
Thuwal 23955-6900, Saudi Arabia
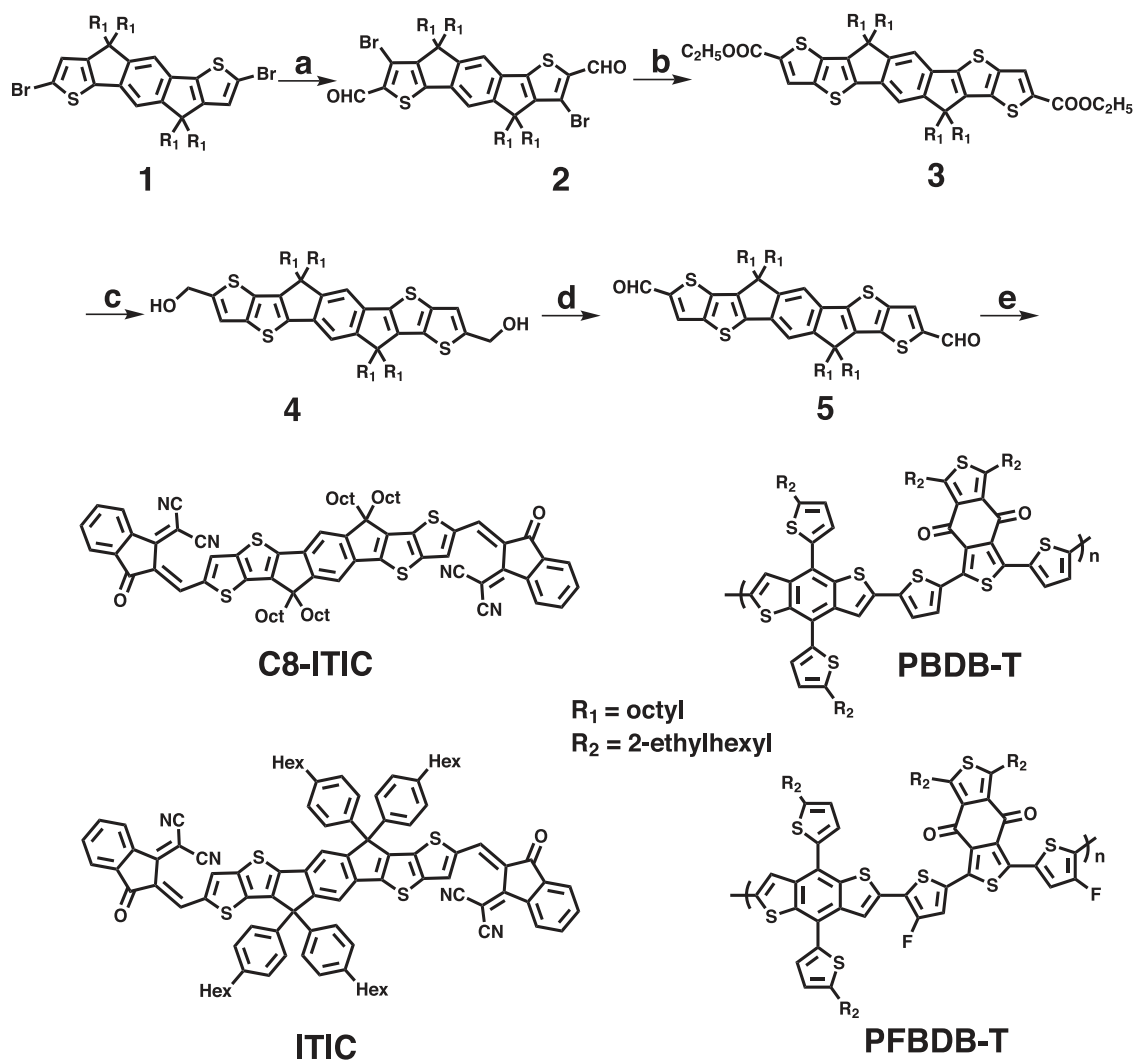
Scheme 1. The synthetic route to C8-ITIC and the structures of ITIC, PBDB-T, and PFBDB-T. a) Lithium diisopropylamide (LDA)/dimethylformamide (DMF)/76%, b) ethyl mercaptoacetate/K_2CO_3/DMF/69%, c) lithium aluminum hydride (LAH)/tetrahydrofuran (THF)/90%, d) Dess–Martin periodinate/THF/85%, e) (3-dihydro-1H-inden-1-ylidene)malononitrile/pyridine/CHCl$_3$/82%.

large impact on the molecular packing, the replacement of these relatively bulky side chains with simple linear alkyl chains could potentially improve the packing ability and the charge transport mobility of these molecules. Although simple conceptually, the synthesis of IDTT with alkyl side chains is challenging since the corresponding trialkyl cations tend to rearrange or eliminate under analogous Friedel–Crafts-type ring closing reactions.[23]

Herein, we report a novel route to prepare an alkylated IDTT-based acceptor {(2Z)-2-[(8-{(E)-1-(Dicyanomethylidene)-3-oxo-1,3-dihydro-2H-inden-2-ylidene]methyl}-6,6,12,12-tetraoctyl-6,12-dihydrothieno[3,2-b]thieno[2″,3″:4′,5′]thieno[2′,3′:5,6]-s-indaceno[2,1-d]thiophen-2-yl)methylidene]-3-oxo-2,3-dihydro-1H-inden-1-ylidene}propanedinitrile (C8-ITIC) (Scheme 1). C8-ITIC shows a red-shifted absorption and higher absorptivity than ITIC. OSC devices based on blends of C8-ITIC and the well-studied donor polymer poly[(2,6-(4,8-bis(5-(2-ethylhexyl)thiophen-2-yl)-benzo[1,2-b:4,5-b′]dithiophene))-alt-(5,5-(1′,3′-di-2-thienyl-5′,7′-bis(2-ethylhexyl)benzo[1′,2′-c:4′,5′-c′]dithiophene-4,8-dione)] (PBDB-T) exhibited better performance than the control devices based on PBDB-T/ITIC, and showed an average PCE of 11.9%. Fluorination of the donor polymer backbone has been shown to be an efficient strategy to improve the PCE of OSCs in many cases.[24] Hence, we also synthesized a new analog of PBDB-T in which the backbone was fluorinated to poly{4,8-bis[5-(2-ethylhexyl)thiophen-2-yl]benzo[1,2-b:4,5-b′]bisthiophene-alt-1,3-bis(2-ethylhexyl)-5-(4-fluorothiophen-2-yl)-7-{5-[tri(propan-2-yl)silyl]thiophen-2-yl}-4H,8H-benzo[1,2-c:4,5-c′]bisthiophene-4,8-dione} (PFBDB-T), Scheme 1). Upon fluorination, PFBDB-T exhibited a deeper highest occupied molecular orbital (HOMO) and a red-shifted absorption spectrum compared to PBDB-T. As a consequence, solar cells based on the blends of PFBDB-T/C8-ITIC demonstrated a high V_{OC} of 0.94 V and a PCE of up to 13.2%, which is among the highest reported PCE of OSCs.

The synthetic route to C8-ITIC is shown in Scheme 1. IDT-dicarbaldehyde **2** was prepared by the base-catalyzed rearrangement of the commercially available IDT monomer **1**, followed by quenching with DMF in a yield of 76%. Subsequent treatment with ethyl mercaptoacetate under basic
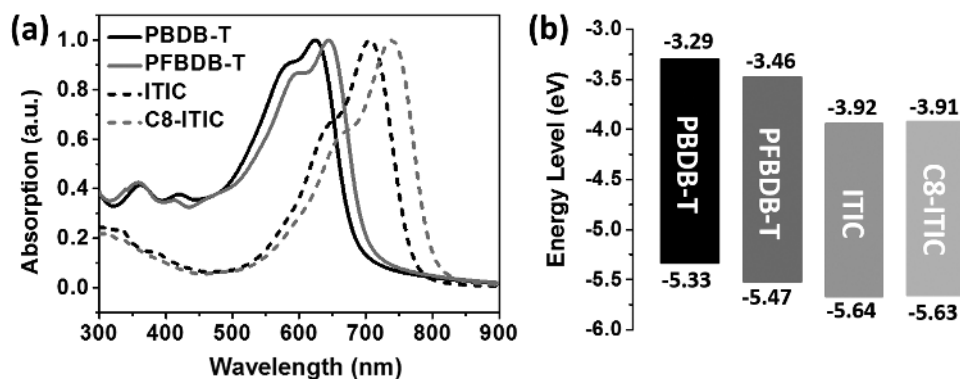
Figure 1. a) Thin film UV–vis absorption spectrum and b) energy levels (calculated from CV) of PBDB-T, PFBDB-T, ITIC and C8-ITIC in drop-cast films.

conditions afforded IDTT-dicarboxylate **3** in 69% yield. The advantage of this route to alkylated IDTT is that all intermediates are soluble and readily purified, in contrast to our previous route in which several intermediates were insoluble and hence difficult to purify and characterize.[23] The ester groups on **3** were readily converted to aldehyde groups via a two-step reduction/oxidation route using LiAlH4, followed by the Dess–Martin periodinate to afford IDTT-dialdehyde **5** in 76% yield over two steps. The final acceptor C8-ITIC was prepared by the Knoevenagel condensation reaction of **5** and IC in a yield of 82%. PFBDB-T was synthesized using a similar synthetic route to PBDB-T (Scheme S1, Supporting Information).[25] PBDB-T and PFBDB-T had number average molecular weights (M_n) of 23 and 26 kDa, and dispersity (Đ) of 2.1 and 2.6, respectively, allowing an accurate comparison of their properties.

The UV–vis absorption spectra of PBDB-T, PFBDB-T, ITIC, and C8-ITC as thin films and in dilute chlorobenzene are shown in **Figure 1**a and in Figure S1 in the Supporting Information. By substitution of the phenylalkyl for linear alkyl side chains, C8-ITIC exhibited a red-shifted absorption maximum at 680 and 738 nm in solution and film, respectively, compared to ITIC. Upon fluorination, PFBDB-T also exhibited a more red-shifted absorption spectrum than PBDB-T, with an absorption maximum of 644 nm in film. The complementary absorption spectra between the donor polymers and acceptor small molecules are beneficial to the broad absorption of OSC blends. Additionally, solution measurements show that C8-ITIC exhibited a higher

absorption coefficient (ε) of 2.05×10^5 M^{-1} cm^{-1} compared to that of ITIC (1.72×10^5 M^{-1} cm^{-1}) (Figure S1 and Table S1, Supporting Information). Both the red-shifted absorption spectra and the higher absorption coefficient indicate that the side chains play an important role on the optical properties of acceptor molecules, both in aggregated (film) and molecular (solution) states. In contrast, the fluorination of the PBDB-T backbone has a negligible effect on the extinction coefficient, with both PBDB-T and PFBDB-T showing an almost identical value of 6.80×10^4 M^{-1} cm^{-1}. Noticeably, temperature-dependent absorption spectra (Figure S2, Supporting Information) show that PFBDB-T has a stronger propensity to aggregate than PBDB-T. The molecular energy levels of the donors and acceptors were measured by cyclic voltammetry (CV). As shown in Figure 1b and Figure S3 (Supporting Information), the HOMO levels of both acceptors were very similar at −5.64 eV for ITIC and −5.63 eV for C8-ITIC. However, fluorination of the polymer was found to result in both deeper HOMO and lowest unoccupied molecular orbital (LUMO) levels (−5.47 and −3.46 eV, respectively).

To investigate the photovoltaic performance of these materials, OSC devices with an inverted device structure of ITO/In2O3/ZnO/active layer/MoO3/Ag (**Figure 2**) based on PBDB-T/ITIC, PBDB-T/C8-ITIC, PFBDB-T/ITIC, and PFBDB-T/C8-ITIC blends were fabricated. The addition of the In2O3 layer between the ITO and ZnO layers leads to a smoothing of the ZnO layer and was found to increase the fill factor (FF) and device reproducibility. Atomic force microscopy images show that the root mean square
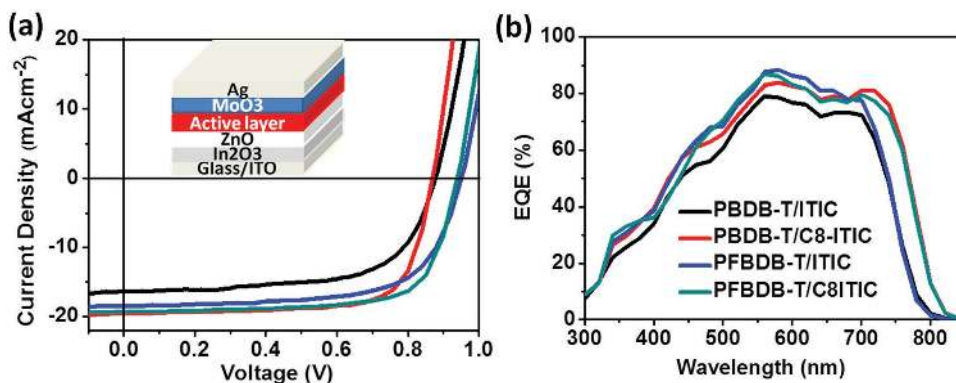

Figure 2. a) J–V curve (device structure inset) and b) EQE curve of PBDB-T/ITIC, PBDB-T/C8-ITIC, PFBDB-T/ITIC, and PFBDB-T/C8-ITIC blend-based OSCs under optimized condition.

    © 2018 The Authors. Published by WILEY-VCH Verlag GmbH & Co. KGaA, Weinheim

**ADVANCED
SCIENCE NEWS**

www.advancedsciencenews.com

**ADVANCED
MATERIALS**

www.advmat.de

Table 1. Summary of optimized OSC devices' performance based on PBDB-T/ITIC, PBDB-T/C8-ITIC, PFBDB-T/ITIC, and PFBDB-T/C8-ITIC blends.

Blends	J_{sc} [mA cm^{-2}]	V_{oc} [V]	FF	PCE [%]
PBDB-T/ITIC[a]	17.1 ± 1.0 (17.0)[b]	0.89 ± 0.005 (0.89)[b]	0.65 ± 0.01 (0.66)[b]	9.9 ± 0.5 (10.0)[b]
PBDB-T/C8-ITIC[c]	19.7 ± 0.6 (19.7)[b]	0.86 ± 0.007 (0.87)[b]	0.70 ± 0.05 (0.73)[b]	11.9 ± 0.4 (12.41)[b]
PFBDB-T/ITIC[c]	17.9 ± 0.4 (18.5)[b]	0.96 ± 0.004 (0.95)[b]	0.67 ± 0.02 (0.66)[b]	11.5 ± 0.4 (11.71)[b]
PFBDB-T/C8-ITIC[c]	19.3 ± 0.7 (19.6)[b]	0.93 ± 0.007 (0.94)[b]	0.69 ± 0.02 (0.72)[b]	12.4 ± 0.4 (13.2)[b]

[a]1:1 (w/w of donor/acceptor), 1,8-diiodooctane (DIO) = 0.5%, 160 °C annealing; [b]Values of device with best performance; [c]1:1.25 (w/w of donor/acceptor).

roughness of the ZnO surface reduced from 1.44 to 0.84 nm upon In$_2$O$_3$ treatment (Figure S4, Supporting Information). The optimized device fabrication conditions and device data of these four blends are shown in Figure 2a and summarized in **Table 1**. Apart from devices based on the PBDB-T/ITIC blend, devices from all other blends exhibited the best OSC performance asspun without any processing additives or annealing processes.

Compared to the control device of PBDB-T/ITIC, the PBDB-T/C8-ITIC-based OSC showed a significantly improved average J_{SC} and FF with a similar V_{OC}, and hence yielded a higher PCE of close to 12%. Interestingly, the addition of processing additives or postdeposition thermal annealing did not further improve the PCE of PBDB-T/C8-ITIC blend-based OSCs (see Table S2 in the Supporting Information). The same improvement for the alkylated acceptor was found in blends with PFBDB-T. In that case, a higher V_{OC} was observed concordant with the higher ionization potential of the fluorinated polymer. The consistently higher J_{SC} and FF of C8-ITIC containing devices may be attributed to its broad absorption spectrum and higher absorptivity. Among these devices, as-cast PFBDB-T/C8-ITIC blend-based OSCs exhibited the best performance with a J_{SC} of 19.6 mA cm^{-2}, a V_{OC} of 0.94 V, an FF of 0.72, and an upper PCE of 13.2% (average PCE over 40 devices: 12.4%). The external quantum efficiency (EQE) measurements (Figure 2b) show that C8-ITIC blends exhibit a broader EQE range than ITIC-based devices, consistent with the UV–vis absorption spectra of the corresponding blends (Figure S5, Supporting Information). The calculated average J_{SC} from the integration of the EQE spectra of PFBDB-T/C8-ITIC-based OSCs is 18.7 mA cm^{-2}, which is well matched with that obtained from the $J–V$ curve.

From the $J–V$ data, it is worth highlighting that a high V_{OC} (0.94 V) can be achieved using PFBDB-T/C8-ITIC, while still maintaining an impressive J_{SC} of around 19.6 mA cm^{-2}. In order to elucidate the origin of these high V_{OC} and J_{SC} values, we performed a voltage loss analysis using electroluminescence (EL) and EQE measurements. The method is based on the reciprocity relation between light absorption and emission

and is described in ref. [26]. Figure S6 in the Supporting Information shows the EQE and EL spectra of all four blends studied, and **Table 2** shows a summary of the extracted voltage losses. There are two material-dependent components to the V_{OC} loss: the so-called absorption broadening loss $\Delta V_{OC,abs}$, which results from the shape of the EQE being less sharp than the unit step function that is assumed in the Shockley–Queisser limit ($V_{OC,sq}$), and the nonradiative recombination loss $\Delta V_{OC,nr}$, which represents the difference between the ideal V_{OC} that the device, with its nonsharp EQE spectrum, could achieve in the radiative limit ($V_{OC,rad}$) and the actual measured V_{OC}. The first voltage loss, $\Delta V_{OC,abs}$, is generally high in OSCs compared to inorganic solar cells, because offsets in HOMO and LUMO energies at the donor/acceptor heterojunction can lead to weakly absorbing charge transfer (CT) states which are strongly red-shifted compared to the absorption onset of either the donor or acceptor alone. Importantly, in the present case, Table 2 shows that the fluorination of the donor leads to a strong reduction in this voltage loss, with a steepening of the absorption edge compared to PBDB-T which is due to the effect of fluorination in lowering the HOMO and LUMO of the donor, thereby reducing the energetic offset with the acceptor. Interestingly, as a result, the $\Delta V_{OC,abs}$ loss is negligible for blends with PFBDB-T. The second voltage loss, $\Delta V_{OC,nr}$, is lower for the devices made with PFBDB-T than those made with PBDB-T, and is lowest of all for the PBDB-T/C8-ITIC devices at 0.33 V. This is comparable with the low nonradiative losses achieved in other devices using small molecular components.[27,28] While the reason for the reduction in the nonradiative losses upon replacing PBDB-T with PBFDB-T and then on replacing ITIC with C8-ITIC is unknown, it may result from improved charge-transport properties in either component, or it may relate to the larger energy gap between the CT state and ground, according to the energy gap law.[29] This is in agreement with a higher observed effective electron mobility and more balanced hole/electron mobility ratio measured by the space-charge-limited current measurement (see Table S3 in the Supporting Information). It is also worth noting that the total energy losses in PFBDB-T/C8-ITIC, $E_g/q–V_{OC}$, are only around 0.60 V (compared to 0.68 for PBDB-T/ITIC). One of the challenges in OSC has been to reduce this voltage loss, while still retaining efficient photocurrent generation. In this case, a very low voltage loss has been achieved while maintaining a high photocurrent generation over a wide spectrum (Figure 2b (EQE)), which shows that efficient charge separation can take place despite a reduced energetic driving force.

Table 2. Voltage loss analysis for the devices based on PBDB-T/ITIC, PBDB-T/C8-ITIC, PFBDB-T/ITIC, and PFBDB-T/C8-ITIC blends.

Donor	Acceptor	E_g/q [V]	$V_{OC,sq}$ [V]	$V_{OC,rad}$ [V]	$\Delta V_{OC,abs}$ [V] (±0.01)	V_{OC} [V]	$\Delta V_{OC,nr}$ [V]
PBDB-T	ITIC	1.57	1.30	1.26	0.03	0.89	0.37
PFBDB-T	ITIC	1.57	1.30	1.30	−0.01	0.96	0.34
PBDB-T	C8-ITIC	1.53	1.26	1.24	0.02	0.86	0.38
PFBDB-T	C8-ITIC	1.53	1.26	1.26	−0.02	0.93	0.33

In order to obtain insights into the behaviors of crystallization and aggregation of donor and acceptor molecules, grazing incidence wide angle X-ray scattering (GIWAXS) was implemented on pure and blend thin films.[30] First, the single-component thin films, namely ITIC, C8-ITIC, PBDB-T, and PFBDB-T, without and with thermal annealing, were measured to examine the crystallization behaviors of each material. From the 2D GIWAXS patterns (see Figure S8 in the Supporting Information), the as-spun C8-ITIC film exhibits sharp and well-defined diffraction spots along the horizontal, vertical and off-axis directions, while as-spun ITIC only exhibits discernible diffraction features along the horizontal and vertical directions. This implies that as-cast C8-ITIC molecules have higher tendency to crystallize in ordered 3D structures, while as-cast ITIC only crystallizes along the three principle crystallographic axis

similar to conjugated polymers.[31] Noticeably, thermal annealing at 160 °C strongly improves the crystallinity of both C8-ITIC and ITIC thin films, evidenced by the abundance of diffraction features in the 2D GIWAXS patterns. It is noteworthy that the ITIC thin film reveals off-axis diffraction after thermal annealing at 160 °C, suggesting that the ITIC molecules can also form a highly ordered arrangement along 3D crystallographic directions with the aid of thermal annealing. Both C8-ITIC and ITIC undergo changes to a different crystal structure with annealing, with the complicated diffraction pattern of C8-ITIC suggesting the presence of multiple polymorphs. The diffraction patterns of the neat donor polymers reveal less ordered structures with broad (h00) and (00l) diffraction peaks along the in-plane direction, and broad (0k0) diffraction peaks along the out-of-plane direction, suggestive of a face-on orientation of crystallites. With
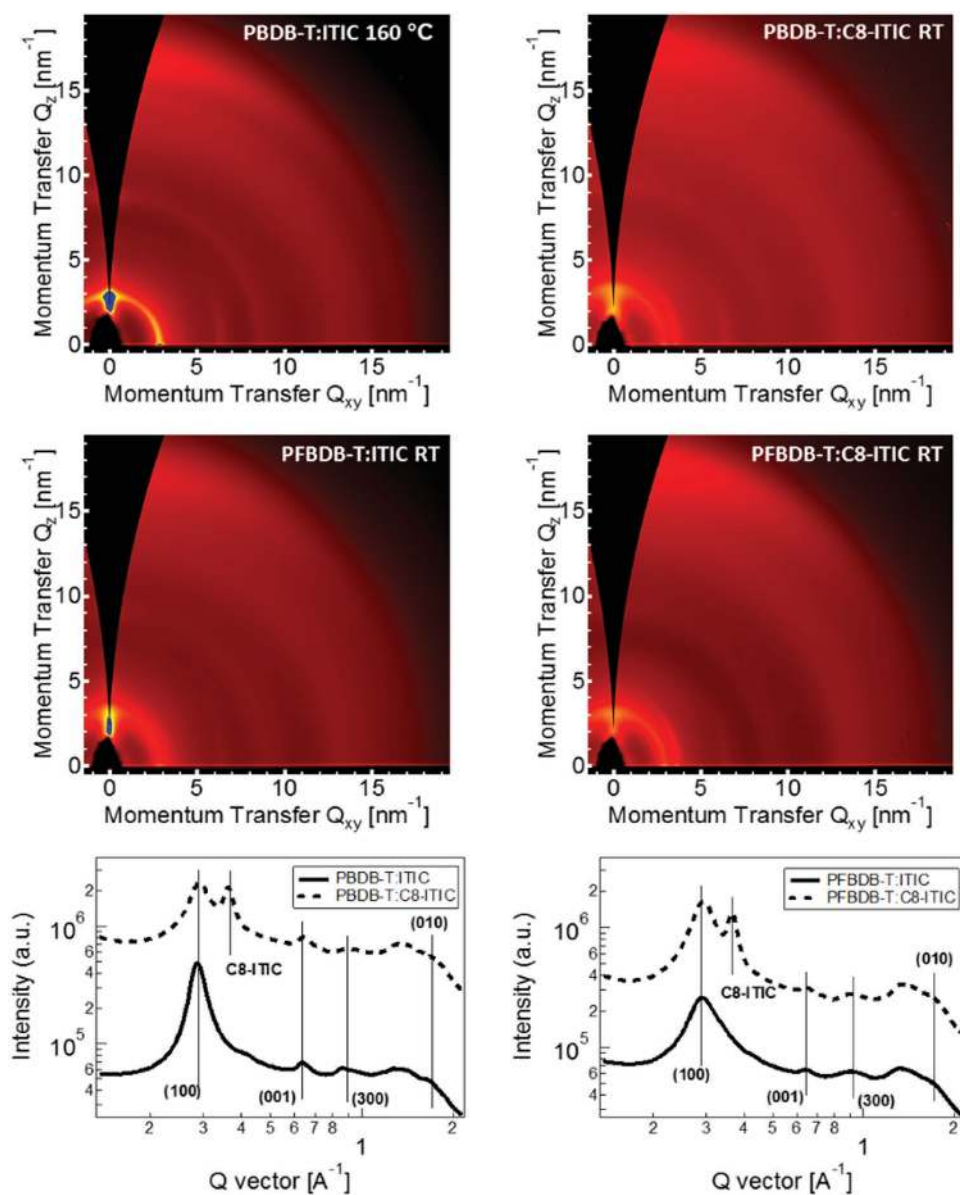

Figure 3. 2D GIWAXS patterns of blends of PBDB-T/ITIC, PBDB-T/C8-ITIC, PFBDB-T/ITIC, and PFBDB-T/C8-ITIC processed under optimized conditions for device performance. Reduced 1D GIWAXS profiles along in-plane direction.

annealing, the polymer order improves without a change in peak positions. The angular distributions of all diffraction peaks for both polymers remain the same after thermal annealing, with slight intensity enhancement.

Intriguingly, the strong crystallization tendency of ITIC and C8-ITIC is largely suppressed when blended with PBDB-T and PFBDB-T. The 2D GIWAXS patterns of the optimized PBDB-T/ITIC, PBDB-T/C8-ITIC, PFBDB-T/ITIC, and PFBDB-T/C8-ITIC blends are dominated by the diffraction features of the donor polymers, as shown in **Figure 3**. To be quantitative, the reduced 1D GIWAXS profiles along the in-plane direction are also plotted in Figure 3. For the ITIC-based blends, only diffraction peaks from the polymer phase are seen with a complete absence of ITIC diffraction features. In contrast, a well-defined peak around $q \approx 0.36$ A^{-1} ($d \approx 1.75$ nm) assigned to C8-ITIC can be recognized in the scattering patterns of the PBDB-T/C8-ITIC and PFBDB-T/C8-ITIC blends. The 1D profiles taken along the out-of-plane direction are shown in Figure S9 (Supporting Information), showing only minor differences. Altogether with the GIWAXS trends of pure ITIC and C8-ITIC, it is found that the crystallization of both ITIC and C8-ITIC is suppressed by the donor polymers in the blends; however, the increased propensity of C8-ITIC to crystallize enables it to retain some molecular order in blends. This improved molecular packing of C8-ITIC compared to ITIC in blends is considered to be a contributing factor for the improved J_{SC} and FF, with improved molecular ordering supporting an increase in charge-transport characteristics and to reduced recombination.

In conclusion, we report the synthesis of a new IDTT-based acceptor, C8-ITIC, with linear alkyl side chains via a hetero-cycle extension strategy. Upon comparison of its properties to a common analog bearing phenylalkyl side chains, we find that alkylation results in a reduction in the optical band gap, higher absorptivity, and an increased propensity to crystallize leading to a higher PCE in bulk heterojunction solar cells employing blends of C8-ITIC with the donor polymer PBDB-T. By preparation of a novel fluorinated analog of PBDB-T, impressive PCEs of up to 13.2% were observed. Electroluminescence studies show that fluorination reduces the energy loss of the blends, with PFBDB-T/C8-ITIC-based cells exhibiting a small energy loss of 0.6 eV despite displaying a high J_{SC} of 19.6 mA cm^{-2} in solar cells.

Supporting Information

Supporting Information is available from the Wiley Online Library or from the author. Additional data relating to this publication can be found at http://dx.doi.org/10.6084/m9.figshare.5364058.

Conflict of Interest

The authors declare no conflict of interest.

[1] W. Chen, Q. Zhang, *J. Mater. Chem. C* **2017**, *5*, 1275.

[2] A. Facchetti, *Mater. Today* **2013**, *16*, 123.

[3] G. Zhang, K. Zhang, Q. Yin, X. F. Jiang, Z. Wang, J. Xin, W. Ma, H. Yan, F. Huang, Y. Cao, *J. Am. Chem. Soc.* **2017**, *139*, 2387.

[4] J. T. Bloking, X. Han, A. T. Higgs, J. P. Kastrop, L. Pandey, J. E. Norton, C. Risko, C. E. Chen, J. L. Brédas, M. D. McGehee, A. Sellinger, *Chem. Mater.* **2011**, *23*, 5484.

[5] Y. Lin, Q. He, F. Zhao, L. Huo, J. Mai, X. Lu, C. J. Su, T. Li, J. Wang, J. Zhu, Y. Sun, C. Wang, X. Zhan, *J. Am. Chem. Soc.* **2016**, *138*, 2973.

[6] L. Yang, S. Zhang, C. He, J. Zhang, H. Yao, Y. Yang, Y. Zhang, W. Zhao, J. Hou, *J. Am. Chem. Soc.* **2017**, *139*, 1958.

[7] Y. Liu, Z. Zhang, S. Feng, M. Li, L. Wu, R. Hou, X. Xu, X. Chen, Z. Bo, *J. Am. Chem. Soc.* **2017**, *139*, 3356.

[8] S. Holliday, R. S. Ashraf, C. B. Nielsen, M. Kirkus, J. A. Rohr, C. H. Tan, E. Collado-Fregoso, A. C. Knall, J. R. Durrant, J. Nelson, I. McCulloch, *J. Am. Chem. Soc.* **2015**, *137*, 898.

[9] S. Holliday, R. S. Ashraf, A. Wadsworth, D. Baran, S. A. Yousaf, C. B. Nielsen, C.-H. Tan, S. D. Dimitrov, Z. Shang, N. Gasparini, M. Alamoudi, F. Laquai, C. J. Brabec, A. Salleo, J. R. Durrant, I. McCulloch, *Nat. Commun.* **2016**, *7*, 11585.

[10] Y. Lin, J. Wang, Z. Zhang, H. Bai, Y. Li, D. Zhu, X. Zhan, *Adv. Mater.* **2015**, *27*, 1170.

[11] T. Liu, X. Xue, L. Huo, X. Sun, Q. An, F. Zhang, T. P. Russell, F. Liu, Y. Sun, *Chem. Mater.* **2017**, *29*, 2914.

[12] H. Bin, Z. G. Zhang, L. Gao, S. Chen, L. Zhong, L. Xue, C. Yang, Y. Li, *J. Am. Chem. Soc.* **2016**, *138*, 4657.

[13] F. Zhao, S. Dai, Y. Wu, Q. Zhang, J. Wang, L. Jiang, Q. Ling, Z. Wei, W. Ma, W. You, C. Wang, X. Zhan, *Adv. Mater.* **2017**, *29*, 1700144.

[14] H. Yao, L. Ye, J. Hou, B. Jang, G. Han, Y. Cui, G. M. Su, C. Wang, B. Gao, R. Yu, H. Zhang, Y. Yi, H. Y. Woo, H. Ade, J. Hou, *Adv. Mater.* **2017**, *29*, 1700254.

[15] W. Zhao, S. Li, H. Yao, S. Zhang, Y. Zhang, B. Yang, J. Hou, *J. Am. Chem. Soc.* **2017**, *139*, 7148.

[16] S. Dai, F. Zhao, Q. Zhang, T.-K. Lau, T. Li, K. Liu, Q. Ling, C. Wang, X. Lu, W. You, X. Zhan, *J. Am. Chem. Soc.* **2017**, *139*, 1336.

[17] Y. Lin, F. Zhao, Q. He, L. Huo, Y. Wu, T. C. Parker, W. Ma, Y. Sun, C. Wang, D. Zhu, A. J. Heeger, S. R. Marder, X. Zhan, *J. Am. Chem. Soc.* **2016**, *138*, 4955.

[18] Y. Yang, Z. G. Zhang, H. Bin, S. Chen, L. Gao, L. Xue, C. Yang, Y. Li, *J. Am. Chem. Soc.* **2016**, *138*, 15011.

[19] J. Wang, W. Wang, X. Wang, Y. Wu, Q. Zhang, C. Yan, W. Ma, W. You, X. Zhan, *Adv. Mater.* **2017**, *29*, 1702125.

[20] Y. Li, L. Zhong, B. Gautam, H.-J. Bin, J.-D. Lin, F.-P. Wu, Z. Zhang, Z.-Q. Jiang, Z.-G. Zhang, K. Gundogdu, Y. Li, L.-S. Liao, *Energy Environ. Sci.* **2017**, *10*, 1610.

[21] W. Wang, C. Yan, T. K. Lau, J. Wang, K. Liu, Y. Fan, X. Lu, X. Zhan, *Adv. Mater.* **2017**, *29*, 1701308.

[22] B. Kan, H. Feng, X. Wan, F. Liu, X. Ke, Y. Wang, Y. Wang, H. Zhang, C. Li, J. Hou, Y. Chen, *J. Am. Chem. Soc.* **2017**, *139*, 4929.

[23] W. Zhang, Y. Han, X. Zhu, Z. Fei, Y. Feng, N. D. Treat, H. Faber, N. Stingelin, I. McCulloch, T. D. Anthopoulos, M. Heeney, *Adv. Mater.* **2016**, *28*, 3922.

[24] N. Leclerc, P. Chávez, O. A. Ibraikulov, T. Heiser, P. Lévêque, *Polymers* **2016**, *8*, 11.

**ADVANCED
SCIENCE NEWS**

www.advancedsciencenews.com

**ADVANCED
MATERIALS**

www.advmat.de

[25] D. Qian, L. Ye, M. Zhang, Y. Liang, L. Li, Y. Huang, X. Guo, S. Zhang, Z. Tan, J. Hou, *Macromolecules* **2012**, *45*, 9611.

[26] U. Rau, *Phys. Rev. B* **2007**, *76*, 85303.

[27] S. M. Tuladhar, M. Azzouzi, F. Delval, J. Yao, A. A. Y. Guilbert, T. Kirchartz, N. F. Montcada, R. Dominguez, F. Langa, E. Palomares, J. Nelson, *ACS Energy Lett.* **2016**, *1*, 302.

[28] D. Baran, T. Kirchartz, B. S. Wheeler, S. Dimitrov, M. Abdelsamie, J. Gorman, R. S. Ashraf, S. Holliday, A. Wadsworth, N. Gasparini, P. Kaienburg, H. Yan, A. Amassian, C. J. Brabec, J. R. Durrant, I. Mcculloch, *Energy Environ. Sci.* **2016**, *9*, 3783.

[29] J. Benduhn, K. Tvingstedt, F. Piersimoni, S. Ullbrich, Y. Fan, M. Tropiano, K. A. McGarry, O. Zeika, M. K. Riede, C. J. Douglas, S. Barlow, S. R. Marder, D. Neher, D. Spoltore, K. Vandewal, *Nat. Energy* **2017**, *2*, 17053.

[30] N. M. Kirby, S. T. Mudie, A. M. Hawley, D. J. Cookson, H. D. T. Mertens, N. Cowieson, V. Samardzic-Boban, *J. Appl. Crystallogr.* **2013**, *46*, 1670.

[31] Z. Fei, L. Chen, Y. Han, E. Gann, A. S. R. Chesman, C. R. McNeill, T. D. Anthopoulos, M. Heeney, A. Pietrangelo, *J. Am. Chem. Soc.* **2017**, *139*, 8094.

1705209 (7 of 7)